3D Numerical simulation of natural gas combustion in a fluidized bed reactor

Ziad Hamidouche, Enrica Masi, Pascal Fede, Olivier Simonin, Renaud Ansart, Salah Dounit, Mehrdji Hemati

22nd FBC JUNE 2015 Turku, Finland

3D Numerical simulation of natural gas combustion in a fluidized bed reactor

Z. Hamidouche[1,3], E. Masi[1,3], P. Fede[1,3], O. Simonin[1,3], R. Ansart[2,3], S. Dounit[2,3], M. Hemati[2,3]

[1] *Université de Toulouse ; INPT, UPS ; IMFT (Institut de Mécanique des Fluides de Toulouse), Allée Camille Soula, 31400 Toulouse, France*
[2] *Université de Toulouse ; INPT, UPS ; LGC (Laboratoire de Génie Chimique), 18 Chemin de la Loge, 31078 Toulouse, France*
[3] *CNRS, Fédération de recherche FERMAT, 31400 Toulouse, France*

Tel.: 05 34 32 29 08, Fax.: 05 34 32 29 94, e-mail address: emasi@imft.fr

Abstract

This study presents detailed 3D unsteady CFD simulations, performed using NEPTUNE_CFD V1.08@Tlse code, of air-methane combustion in a dense fluidized bed containing inert particles. Predictions are compared with the experimental data reported in Dounit et al. (2001a, 2001b, 2008). In their study, the authors investigated the behavior of natural gas combustion process in dense fluidized bed and in the freeboard at temperatures lower than a critical value (< 850°C). The main outputs of the experiments are vertical profiles of gaseous-species concentrations and gas temperature. In CFD simulations, an Euler-Euler approach is used to compute separately gas and solid phases flows (primary variables for each phase are volume fraction, velocity, enthalpy, mass fraction), with detailed closure models to account for fluid-particle and particle-particle mass, momentum and energy transfers. Gaseous combustion is modeled by a two-step mechanism following Arrhenius-type equations (Dryer & Glassman, 1973, Westbrook and Dryer, 1981). The Eulerian modeling takes into account the energy exchange by radiation between the gas, the particles and the reactor walls as well. The 3D unsteady simulations are analyzed to characterize dynamic flow behavior, thermal spatial distribution and interphase equilibrium. Time-averaged quantities are computed to compare predictions with the available experimental measurements.

1 Introduction

Fluidized-bed reactors in which combustion takes place at relatively low temperature have the main advantage to minimize combustion pollutants. They are used in many industrial applications, especially in solid treatment applications where energy may be supplied by direct combustion of fossil fuels inside the bed itself. Natural gas is the least polluting fossil fuel and, when burnt at low temperatures, it involves lower pollutant emissions, especially NO and NO_2. Understanding and mastered natural gas combustion process in fluidized beds is thus of great interest with respect to environmental issues. The present study is a theoretical/numerical investigation of the air-methane combustion in a dense fluidized-bed reactor for which experimental results are available by the works of Dounit et al. (2001a, 2001b, 2008). The experimental setup consisted of a reactor of 180 mm in diameter and 1400 mm in height, above which, a disengagement section of 360 mm in diameter is added. The experiments were conducted using sand particles with mean diameter 350 µm and density 2650 kg/m^3. In order to maintain a constant temperature in the bed, cooling air is made circulate in a double shell. A detailed description of the experiments may be found in the aforementioned publications.

2 Euler-Euler model for collisional reactive flows

Interactions between particles of the same diameter and a gas mixture composed of N species are predicted in a Eulerian framework using the two-fluid model formalism. Such an approach involves two separate sets of equations (one for each phase) including mass, momentum and enthalpy transport equations. In addition, and uniquely for the gas phase, a set of N-1 species equations and a state law are used for predicting the species evolution and the change in gas density. Particle and gas phases are coupled through interphase transfer terms. A description of the modeling is given in the present section. More details can be found elsewhere (Simonin and al., 1993, Simonin 2000).

2.1 *Mass, momentum and enthalpy transport equations*

The system of equations describing the evolution of the mean mass, momentum and enthalpy quantities is written, for each phase, as follows:

$$\frac{\partial}{\partial t}(\alpha_k \rho_k) + \frac{\partial}{\partial x_j}\left(\alpha_k \rho_k U_{k,j}\right) = 0 \tag{1}$$

$$\alpha_k \rho_k \left[\frac{\partial U_{k,i}}{\partial t} + U_{k,j}\frac{\partial U_{k,i}}{\partial x_j}\right] = -\alpha_k \frac{\partial P_g}{\partial x_i} + \alpha_k \rho_k g_i \;\; + \mathrm{I}_{k'\to k,i} - \frac{\partial \Sigma_{k,ij}}{\partial x_j} \tag{2}$$

$$\alpha_k \rho_k \left[\frac{\partial H_k}{\partial t} + U_{k,j}\frac{\partial H_k}{\partial x_j}\right] = \frac{\partial}{\partial x_j}\left(\alpha_k \rho_k K_k \frac{\partial H_k}{\partial x_j}\right) + \; \Pi_{k'\to k} + \; S_{rad_k} \tag{3}$$

In the mass equation (1), α_k represents the volume fraction of the phase k (which may be either the gas, $k = g$, in that case $k' = p$, or the particulate phase $k = p$, in that case $k' = g$); ρ_k and $U_{k,j}$ are phase's density and velocity respectively. In the momentum equation (2), P_g is the gas pressure and g_i the gravity. The term $\mathrm{I}_{k'\to k,i}$ accounts for the interfacial momentum transfer between the phases while the last term in the equation is the transport due to the velocity fluctuations. It is written in terms of the effective stress tensor $\Sigma_{k,ij} = \alpha_k \rho_k R_{k,ij} + \Theta_{k,ij}$. The quantities $R_{k,ij}$ and $\Theta_{k,ij}$ are either the turbulent-Reynolds and the viscous stress tensors for the gas phase $(k = g)$, or the kinetic and the collisional stress tensors for the dispersed phase $(k = p)$. Details concerning their closures as well as the closure of the momentum transfer may be found in Boëlle et al. (1995) and Gobin and al. (2003). Frictional forces were not accounted for since the mean particle volume fraction in the bed was found to not exceed the value of 0.55. In the enthalpy equation (3), H_k represents the total enthalpy of the phase k, which is not affected by the reaction. The first term on the right hand side (r.h.s.) represents the transport of the enthalpy by velocity fluctuations: it is modeled using a Boussinesq approximation through an effective thermal diffusivity K_k (Konan et al., 2010a, 2010b). Such a thermal diffusivity is composed of two contributions: for the gas phase they are the laminar and the turbulent thermal diffusivity coefficients, $K_g = K_g^L + K_g^T$. For the particulate phase, the two contributions are the thermal diffusivity due to the particle agitation and that related to the heat transfer due to the radiation between particles, $K_p = K_p^T + K_p^R$; the latter contribution is neglected in the present work. The second term on the r.h.s. of Eq. (3) accounts for the heat exchange between gas and particulate phases. It is modeled as:

$$-\Pi_{p\to g} = \; \Pi_{g\to p} = -\frac{\alpha_p \rho_p C_{p_p}}{\tau_{gp}^T}\, T_r \tag{7}$$

where $T_r = T_p - T_g$ is the relative temperature et τ_{gp}^T the characteristic mean thermal particle response time scale defined as:

$$\frac{1}{\tau_{gp}^{T}} = \frac{6\lambda_p}{\rho_p C_{p_p}} \frac{\langle Nu \rangle_p}{d_p^2} \tag{8}$$

The Nusselt number is defined as $\langle Nu \rangle_p = 2 + 0.55 Re_p^{1/2} Pr^{1/3}$ where $Re_p = \alpha_g \langle |\overrightarrow{V_r}| \rangle_p \, d_p / \nu_g$ is the mean particle Reynolds number and $Pr = \rho_g \nu_g C_{p_g} / \lambda_g$ is the Prandtl number. C_{p_k} is the phase specific heat. Finally the last term in Eq. (3), S_{rad_k}, accounts for the heat exchange due to thermal radiation in the reactor. Its model is given in Section (2.4).

2.2 *Methane-air mixture combustion modeling*

The first kinetic scheme retained for the methane combustion is a global two-step mechanism proposed by Dryer and Glassman (1973):

$$CH_4 + {}^3/_2 \; O_2 \rightarrow CO + 2\, H_2O \tag{9}$$

$$CO + {}^1/_2 \; O_2 \rightarrow CO_2 \tag{10}$$

The reaction rates are modeled by two Arrhenius-type equations:

$$R_{1DG} = 10^{13.2} \exp\left(-\frac{48.4 \times 4.18 \times 10^3}{R_g T_g}\right) [CH_4]^{0.7} [O_2]^{0.8} \times 10^{-3} \tag{11}$$

$$R_{2DG} = 10^{14.75} \exp\left(-\frac{43 \times 4.18 \times 10^3}{R_g T_g}\right) [CO] [O_2]^{0.25} [H_2O]^{0.5} \times 10^{-4.5} \tag{12}$$

The second kinetic scheme used for the numerical simulation is that proposed by Westbrook and Dryer (1981). It is also based on a two-step mechanism, which is however corrected by introducing a reverse reaction for the carbon monoxide in order to improve the predictions of the heat reaction and to properly reproduce the pressure dependence of the molar-concentration ratio between carbon monoxide and carbon dioxide. The mechanism is modeled by the following reaction rates:

$$R_{1WD} = 2.8 \times 10^9 \exp\left(-\frac{48.4 \times 4.18 \times 10^3}{R_g T_g}\right) [CH_4]^{-0.3} [O_2]^{1.3} \tag{13}$$

$$\begin{aligned} R_{2WD} = {} & 10^{14.6} \exp\left(-\frac{40.0 \times 4.18 \times 10^3}{R_g T_g}\right) [CO] [O_2]^{0.25} [H_2O]^{0.5} \times 10^{-4.5} \\ & - 5 \times 10^8 \exp\left(-\frac{40.0 \times 4.18 \times 10^3}{R_g T_g}\right) [CO_2] \end{aligned} \tag{14}$$

R_{1DG}, R_{2DG}, R_{1WD} and R_{2WD} have units of $\mathrm{mol/m^3/s}$ and the species molar concentrations are given in $\mathrm{mol/m^3}$. In the numerical simulations, regardless of the kinetic mechanism that is used, $\mathrm{N} = 6$ species are retained for the combustion, they are: methane, oxygen, nitrogen, carbon dioxide, carbon monoxide and water vapor.

2.3 *Balance of gas mixture species*

In order to ensure global mass conservation, the evolution of the species forming the gas mixture was predicted using $\mathrm{N} - 1$ (rather than N dependent species) transport equations:

$$\alpha_g \rho_g \left[\frac{\partial Y_\alpha}{\partial t} + U_{g,j} \frac{\partial Y_\alpha}{\partial x_j}\right] = \frac{\partial}{\partial x_j}\left(\alpha_g \rho_g D_g \frac{\partial Y_\alpha}{\partial x_j}\right) + \Psi_\alpha \tag{15}$$

In Eqs. (15) Y_α represents the mass fraction of the species while D_g is the turbulent diffusion coefficient. The last r.h.s. term accounts for the change in species mass fraction due to the reactions. Such a source term is equal to zero if atomic instead of species mass fractions are computed, since

atomic species are always conserved during any chemical process. For this reason, in this study it was decided to transport the atomic mass fractions of the atomic species C, H and N for which $\Psi_C = \Psi_H = \Psi_N = 0$. They are related to the mass fractions of the mixture gas species by the following relations $\mathrm{Y}_C = 12/16 Y_{CH_4} + 12/28 Y_{CO} + 12/44 Y_{CO2}$, $\mathrm{Y}_H = 4/16 Y_{CH_4} + 2/18 Y_{H_2O}$, $\mathrm{Y}_N = Y_{N2}$. The remaining two species computed by the numerical simulation are CH_4 and CO. According with reactions (11) or (13), the vanishing rate of methane (in $\mathrm{kg/m^3/s}$) is modeled as $\Psi_{CH_4} = -\alpha_g \times W_{CH_4} R_1$. The rate of change of the carbon-monoxide mass fraction has instead to account for both appearance and vanishing of such a species due to reactions (11) and (12), or (13) and (14), respectively. This leads to write the source term as $\Psi_{CO} = \alpha_g \times W_{CO}(R_1 - R_2)$. The unknown carbon dioxide and water vapor mass fractions (Y_{CO_2}, Y_{H_2O}) are deduced from transported species while the oxygen mass fraction is computed according to the conservation law $\mathrm{Y}_{O_2} = 1 - \sum_{\alpha=1}^{\mathrm{N}-1} Y_\alpha$. The gas variable-density should then be related to the computed species mass fractions through the gas temperature and the reference pressure within the reactor and its value updated according with the ideal gas law:

$$\rho_g = \frac{P_{ref}\, W_g}{R_g T_g} = \frac{P_{ref}}{R_g T_g} \left[\sum_{\alpha=1}^{\mathrm{N}} \frac{Y_\alpha}{W_\alpha} \right]^{-1} \tag{16}$$

where W_g is the gas molar mass. The gas specific heat is computed according to the expression $C_{p_g} = \sum_{\alpha=1}^{N} Y_\alpha \; C_{p_\alpha}$.

2.4 *Thermal radiation model*

Concerning the gas phase, the thermal radiation model used in this study (Barlow et al. 2001) assumes that the medium is optically thin enough to allow each radiating point to have an unobstructed isotropic view of the surrounding cold; under such an assumption, the radiation heat loss rate per unit volume may be written as follows:

$$S_{rad_g} = 4\sigma \sum_{\alpha=1}^{n} P_\alpha \beta_\alpha \, \epsilon_{bulk} (T_{bulk}^4 - T_g^4) \; ; \tag{17}$$

where $\sigma = 5.669 \times 10^{-8} \mathrm{W/m^2/K^4}$ is the Stefan-Boltzmann constant; P_α is the partial pressure of the α^{th} species in atmospheres units (mole fraction times local pressure); β_α is the Planck mean absorption coefficient of the α^{th} species; n is the number of species included in the radiation calculation; T_g is the local mean gas temperature and T_{bulk} and ϵ_{bulk} are the surrounding medium temperature and emissivity, respectively. T_{bulk} is either the local mean particle temperature T_p or the temperature of the reactor wall, T_W , according to a critical value of the solid volume fraction. In this study, we set:

$$(T_{bulk}, \epsilon_{bulk}) = \begin{cases} (T_p, \epsilon_p) & \text{if } \alpha_p \geq 0.02 \\ (T_W, \epsilon_W) & \text{otherwise} \end{cases} \tag{18}$$

ϵ_p and ϵ_W are the particles and the wall emissivities, respectively. The four species retained for the calculation are steam, carbon dioxide, carbon oxide and methane (H_2O , CO_2 , CO , CH_4). Their absorption coefficients are made varying as a function of the gas temperature according to the curve fits proposed in the literature (Grosshandler, 1993, Barlow et al., 2001, Sandia TNF web site). Concerning the solid phase, only dilute regions ($\alpha_p \leq 0.02$) were assumed to be affected by the heat loss through particles' radiation toward the reactor walls. For such regions, the related heat loss rate per unit volume was computed as:

$$S_{rad_p} = 4\sigma \beta_p \epsilon_W (T_W^4 - T_p^4) \tag{19}$$

where β_p is the particle absorption coefficient, $\beta_p = \frac{3}{2} \epsilon_p \alpha_p d_p$.

3 Numerical simulations

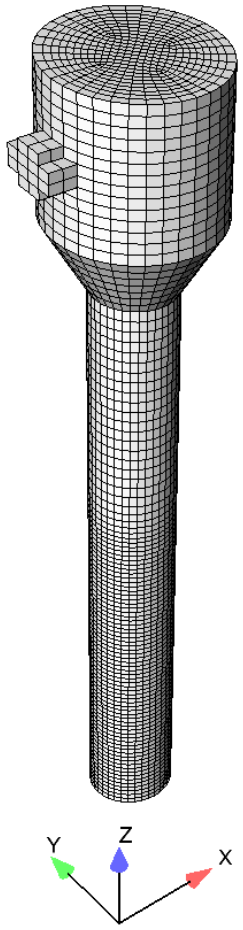

Figure 1. Reactor mesh.

Chemical species	$Cp\ (J/mol/K)$	$\Delta H_f^0\ (kJ/mol)$
CH_4	35.796	−74.8
H_2O	35.744	−241.82
CO_2	39.089	−393.52
CO	29.195	−110.58
O_2	29.426	0
N_2	29.173	0

Table 1. Species thermodynamic properties at standard conditions.

Case	Reaction	Bed Temperature	Number of cells
DG_700_MESH0	Eqs. (11)-(12)	700 °C	31185
DG_700_MESH1	Eqs. (11)-(12)	700 °C	45979
WD_700_MESH1	Eqs. (13)-(14)	700 °C	45979

Table 2. Simulation cases.

Solid phase		Gaseous phase	
Solid mass	12 kg	$Y_{CH_4} = Y_{CO} = Y_C = Y_H$	0
Initial distribution (α_p)	0.55	Y_N	0.8062

Table 3. Initial conditions.

Unsteady three dimensional numerical simulations of the fluidized-bed reactor have been carried out using a Eulerian n-fluid modeling approach for gas-solid turbulent polydisperse flows developed and implemented by IMFT (Institut de Mécanique des Fluides de Toulouse) in the NEPTUNE CFD V1.08@Tlse version. NEPTUNE CFD is a multiphase flow software developed in the framework of the NEPTUNE project, financially supported by CEA (Commissariat à l´Energie Atomique), EDF (Electricité de France), IRSN (Institut de Radioprotection et de Sûreté Nucléaire) and AREVA-NP. The numerical solver has been developed for High Performance Computing (Neau et al., 2013). The Eulerian modeling used in this work was described in Section (2). One class of particle was simulated, with a particle diameter $d_p = 350\ \mu\text{m}$. The latter represents the average sample size used in the experiments (the particle diameter in the sample ranges between $315\ \mu\text{m}$ and $400\ \mu\text{m}$ (Dounit et al., 2001b)). Other quantities of interest for the numerical simulation are the particle mass density $\rho_p = 2650\ \text{kg/m}^3$, the particle emissivity $\epsilon_p = 0.6$, and the particle restitution coefficient, $e_c = 0.9$, which accounts for particle energy exchanges in (partially elastic) collisions. The fluidizing gas is a mixture composed of methane and air injected at the following operating conditions: pressure= $1\ \text{bar}$, total flow rate= $14.6\ \text{Nm}^3/\text{h}$, air factor=1.2 and fluidizing velocity=$2U_{mf}$ at $298\ \text{K}$. In the experiments, a distributer composed of a perforated plate with 0.4% porosity is used. In the numerical simulations, its effect is reproduced by assuming a perfect air-methane mixing at the reactor inlet. Such an assumption is justified by the fact that the pressure drop induced by the distributer is comparable to that induced by the particle bed (which suggests a uniform gas distribution at the reactor inlet). Three different simulations were performed. In all simulations the temperature of the bed was initialized at $700\ ℃$. The

	BC type		Flow rate	Enthalpy		Scalars
	Gas	**Solid**	**Gas**	**Gas**	**Solid**	**Gas**
Reactor bottom	Inlet	Wall	0.00505 kg/s	-231410 J/kg	Null flux	$Y_{CH_4} = 0.0461$, $Y_{CO} = 0$, $Y_N = 0.7319$ $Y_C = 0.034575, Y_H = 0.011525$
Reactor top	Free outlet	Free outlet	Free outlet	Null flux	Null flux	Null flux
Reactor walls	Friction	No slip	-	Null flux	Null flux	Null flux

three simulations differ each other for the grid refinement and the kinetic mechanism. Two types of meshes were employed: a first mesh referred to as MESH0 composed of 31185 cells of dimensions

Table 4 – Boundary conditions

$\Delta_{xmax} = 0.82$ cm, $\Delta_{ymax} = 1.56$ cm, $\Delta_z = 2.5$ cm; a second mesh more refined, referred to as MESH1, composed of 45979 cells of the same dimensions in x and y directions as MESH0 and $\Delta_z = 1.25$ cm for $z < 0.8\,m$ and $\Delta_z = 2.5$ cm for $z > 0.9\,m$ with gradual connection for $0.8\text{ m} < z < 0.9\,m$. No-slip condition for the mean particle velocity, combined with zero-flux condition for the particle fluctuant kinetic energy, are used because found to be satisfactory effective boundary conditions in dense fluidized beds (Fede et al., 2011) for spherical particles bouncing on a very rough wall (or for particles with very irregular shapes bouncing on a frictional flat wall). A summary of the properties of chemical species, simulations cases, initial and boundary conditions are given in Tables (1)-(4). A sketch of the reactor geometry realized using the grid MESH1 is shown in Figure (1).

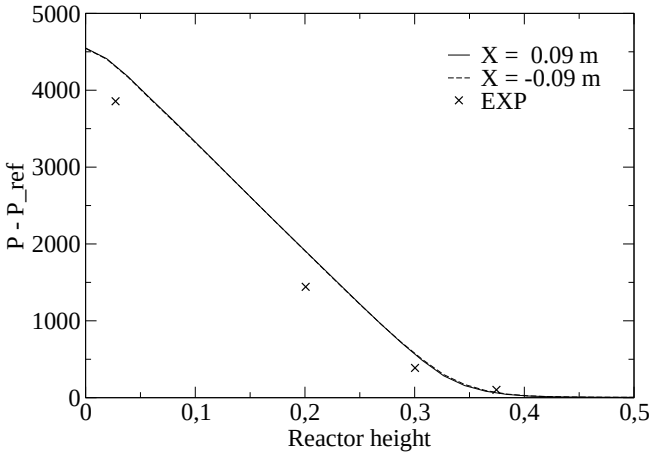

Figure 2. DG_700_MESH0: numerical against experimental mean pressure drop (Pa)

4 Results and discussions

Results obtained for the case DG_700_MESH0 are first analyzed. The numerical simulation has been made run for 80 seconds in order to ensure to reach a permanent regime. In such a regime, particles' and fluid properties are supposed to be statistically stationary and mean (time-averaged) quantities may be retained for comparisons. Figure (2) shows numerical results against experimental measurements of the mean pressure drop along the reactor axis. Globally, the pressure-drop behavior is well reproduced. The difference observed (and estimated to be around 5 %) may be due to the elutriation phenomenon and to the uncertainty in experimental measurements. Numerical against experimental results about the gas temperature in the reactor are shown in Figure (3). In the experiments, the temperature is measured by means of temperature sensors located at several

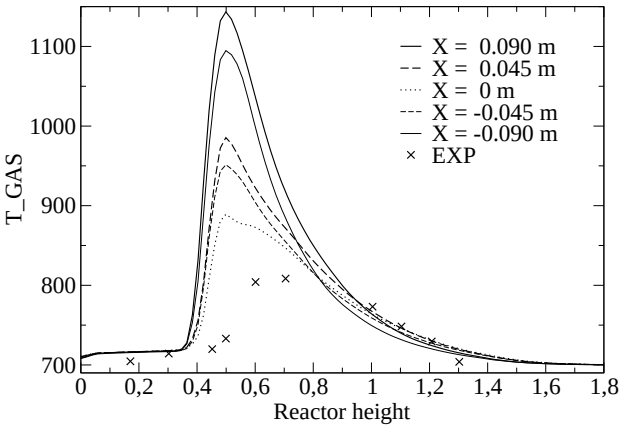

Figure 2 DG_700_MESH0: numerical against experimental mean gas temperature (°C)

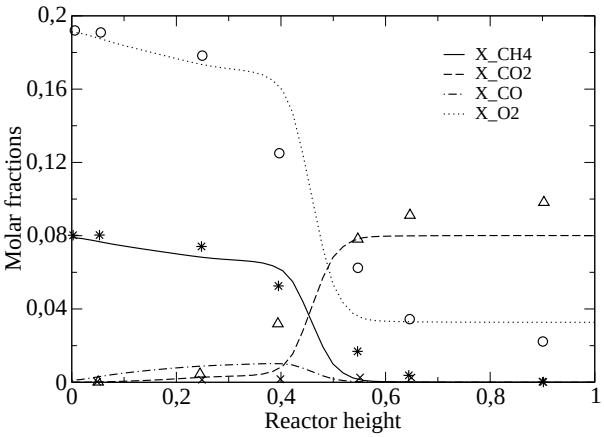

Figure 3. DG_700_MESH0: numerical (lines) against experimental (symbols) mean molar fractions

reactor heights, near the wall. This quantity represents one of the most relevant ones in the fluidized-bed combustor and it needs to be carefully investigated. In their previous studies, Pre et al. (1998) and Dounit et al. (2001a, 2001b, 2008) showed that the combustion zone moves in the reactor depending on the temperature of the dense bed. In particular they showed that for temperatures higher than 800°C the combustion mainly takes place into the bed, while for temperature lower than 800°C, the combustion zone moves towards the freeboard region and over. At the operating point of 700°C, one expects that most of the combustion is in the freeboard region. This is indeed what observed looking at the results illustrated in Figure (3). However, it is worth of note that the numerical simulation overestimates the gas temperature in this region while its predictions are quite accurate into the bed. Further, the temperature-gas predictions are not radially homogeneous and an important difference is observed between the reactor center (X=0 m) and the walls (X±0.09 m, as an example). This may be due to the relatively short simulation time. Comparisons between numerical results and experimental measurements of the species molar fractions are given in Figure (4). In the experiments, gas samples are taken at the center of the reactor using sampling tubes connected to the cooling unit in order to eliminate the steam. Species molar fractions are then measured by means of infrared or paramagnetic type analyzers depending on the species. One can observe that oxygen and carbon dioxide, as predicted by the numerical simulation, do not match the experimental values at the exit. This is due to the fact that in the numerical simulation pure methane was taken into account while, in the experiments, natural gas with 97% methane content was used. The presence of small quantities of

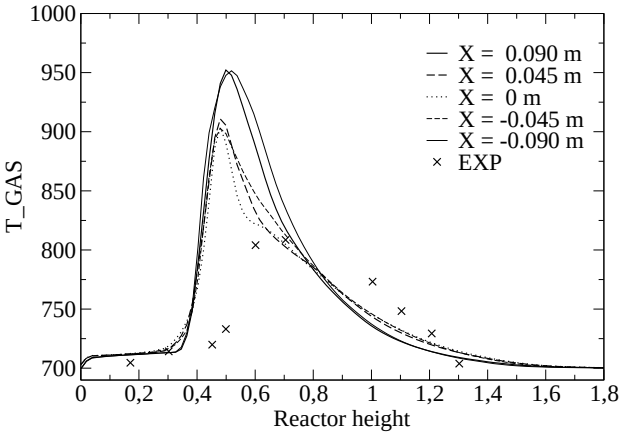

Figure 5. DG_700_MESH1 : numerical against experimental mean gas temperature (°C)

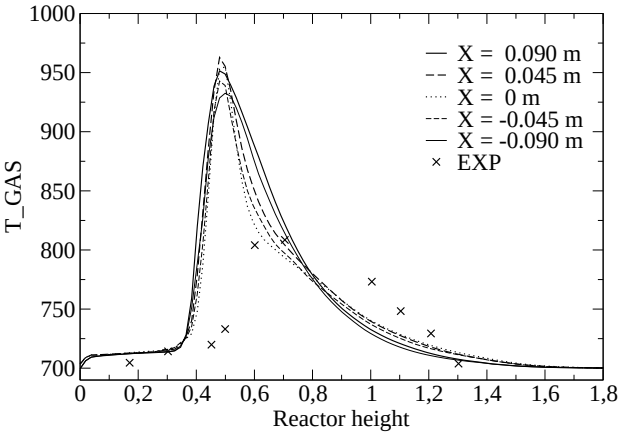

Figure 6. WD_700_MESH1 : numerical against experimental mean gas temperature (°C)

hydrocarbons such as ethane, propane, butane is sufficient to explain the difference observed in molar

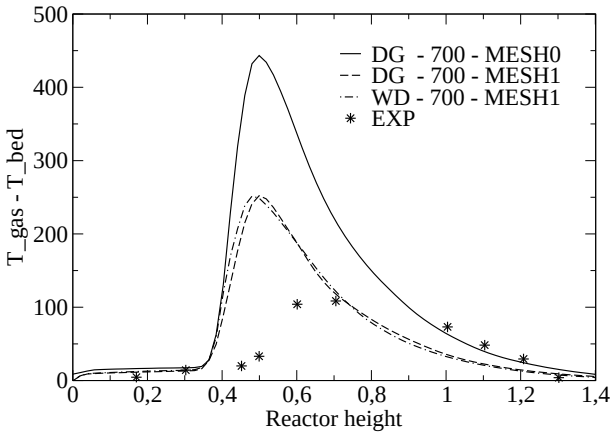

Figure 7. All simulations: numerical against experimental mean gas temperature (°C)

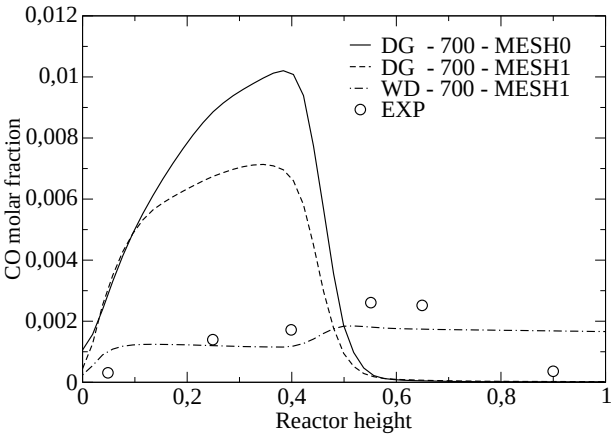

Figure 8. All simulations: numerical against experimental carbon monoxide molar fractions

fraction of reaction products. Otherwise, results of the numerical simulations show that the methane molar fraction is quite well reproduced into the bed while it is underestimated in the freeboard region. These results are consistent with the observations about the gas-temperature overestimate at the freeboard. In this region, the methane conversion is faster compared to the experimental measurements. In order to understand the reasons of such a difference, two additional cases were simulated. A first case, referred to as DG_700_MESH1, in which the mesh of the reactor was refined, and a second case, referred to as WD_700_MESH1, in which the kinetic mechanism of Westbrook and Dryer (1981) together with the finest grid were instead retained. The temperature-gas predictions of these two additional cases are illustrated in Figures (5) and (6). Comparing Figure (5) with Figure (3) one can observe that the numerical predictions are definitely improved using a refined grid. Compared coarser and finest-mesh results, a large difference between the maximum of the temperatures near the wall is observed (about 200 °C). No significant difference is instead noticed compared coarser and finest-grid results about the predictions of the species molar fractions (not shown). The kinetic-mechanism effect on the gas-temperature predictions may be assessed by comparing Figures (5) and (6). Globally, the two models yield similar temperature profiles; nevertheless, the mechanism of Westbrook and Dryer leads to more homogeneous values in the radial direction at each reactor station. A comparison between mean gas temperatures as obtained from all numerical simulations is given in Figure (7). The main difference between the two kinetic mechanisms selected in this study relies on the way to model production/destruction of the carbon monoxide. This species is in fact differently reproduced by the two kinetic models; in particular, it is overestimated by the Dryer and Glassman mechanism within the bed and at the bed surface as illustrated by Figure (8). Moreover its predictions are even more overestimated if a coarser grid is used. As a direct consequence of the better prediction, in the bed, of the carbon monoxide molar fraction as modeled by the Westbrook and Dryer mechanism, a slight improvement of the accuracy of the other species involved in the reaction is observed, as illustrated in Figure (9). However, it is observed that this model leaves unreacted carbon monoxide above the freeboard region. The effect of the mesh size on the bed hydro-thermodynamics may also be observed by Figure (10) in which snapshots of the instantaneous gas-temperature and particle volume fractions for two different grid sizes are shown. Results give the evidence that a better resolution of the bed hydrodynamics has a strong effect on the bed temperature predictions as well.

5 Conclusion

In this study, unsteady 3D numerical simulations of the air-methane combustion in a fluidized-bed reactor containing inert particles were carried out. Numerical simulations were performed using a two-fluid model, which computes separately gas and solid phases flows in a Eulerian framework. Two

distinct combustion mechanisms (Dryer & Glassman, 1973, Westbrook and Dryer, 1981) were tested over two different grids in order to investigate the influence of the kinetics and of the mesh size on the numerical predictions. Time-averaged results were compared with the experimental measurements available in the literature (Dounit et al., 2001a, 2001b, 2008). Results showed that the mechanism of Westbrook and Dryer leads to more homogeneous results of the gas temperature in the radial direction and improves the predictions of the carbon monoxide in the dense bed. But most important, results showed that the gas-temperature predictions are definitely improved if a refined grid is used. This is not the case for the predictions of the species molar fractions. It is conjectured that a finest mesh matches better the hydrodynamics of the bed making it possible to reproduce the bubble-eruption zone at and above the bed surface more accurately. Not enough accurate predictions of the particle volume fraction in such a zone may dramatically affect the gas temperature predictions. This point is crucial and deserves to be further investigated. A mesh sensitivity analysis for different operating points and sample sizes will be conducted as a future work.

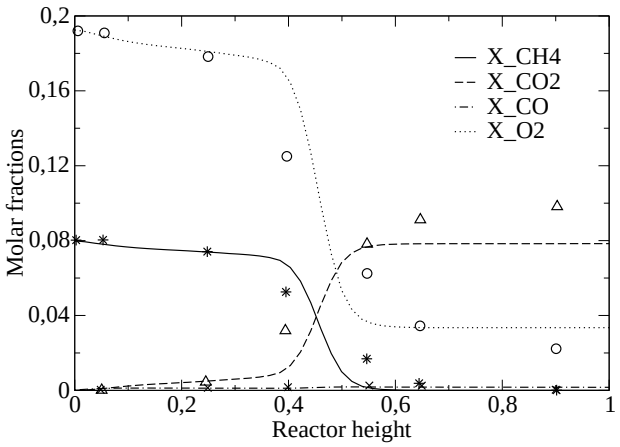

Figure 9. WD_700_MESH1: numerical against experimental mean molar fractions

Acknowledgements This work received funding from the European Community through the SUCCESS project under the 7th Framework program (Grant agreement No. 608571). It reflects only the author's views and the Community is not liable for any use that may be made of the information contained therein. This work was granted access to the HPC resources of CALMIP supercomputing center under the allocation 2015-0111. CALMIP is gratefully acknowledged.

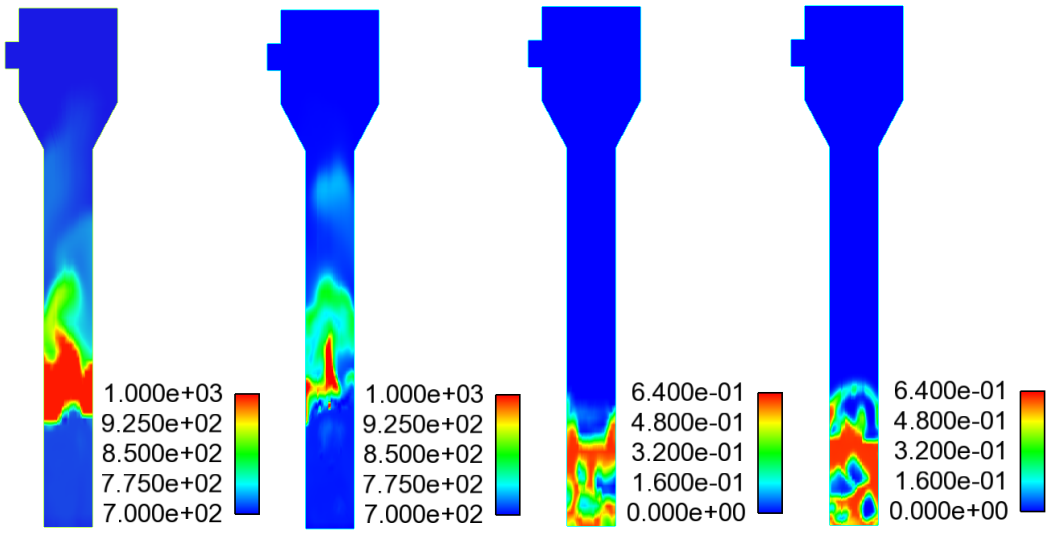

Figure 10. Snapshots at time = 64 seconds of, from the left to the right, DG_700_MESH0 instantaneous gas temperature (°C), DG_700_MESH1 instantaneous gas temperature (°C),

DG_700_MESH0 instantaneous particle volume fraction, DG_700_MESH1 instantaneous particle volume fraction.

6 References

[1] S. Dounit, M. Hemati, D. Steinmetz, Natural gas combustion in fluidised bed reactors between 600 and 850 °C: experimental study and modelling of the freeboard, *Powder Tech*., 120, 49-54, 2001a.

[2] S. Dounit, Combustion of natural gas in fluidised bed reactor: experimental study and modelling of dense and disengagement zones, *Phd Thesis*, INPT, 2001b.

[3] S. Dounit, M. Hemati, R. Andreux, Modelling and experimental validation of a fluidized-bed reactor freeboard region: Application to natural gas combustion, *Chem. Eng. J.,* 140, 457-465, 2008.

[4] F.L. Dryer, I. Glassman, High temperature oxidation of CO and CH4, *14th Symp. Int. Combustion*, 14, 987-1003, 1973.

[5] C.K. Westbrook and F.L. Dryer, Simplified reaction mechanisms for the oxidation of hydrocarbon fuels in flames, *Combust. Sci. Technol*., 27, 31-43, 1981.

[6] O. Simonin, E. Deutsch and J.P. Minier, Eulerian prediction of the fluid/particle correlated motion in turbulent two-phase flows, *Applied Scientific Research*, 51, 275-283, 1993.

[7] O. Simonin, Statistical and continuum modelling of turbulent reactive particulate flows*, Von Karman Institute for Fluid Dynamics*, Rhode Saint Genèse, Belgium, 2000.

[8] Fede, P., Simonin, O., Ansart, G., Neau, H., Ghouila, I., Effect of Wall Boundary Conditions and Mesh Refinement on the Numerical Simulation of a Pressurized Dense Fluidized Bed for Polymerization Reactor, *Proc. of the 10th Int. Conference on Circulating Fluidized Beds and Fluidization Technology*, CFB10, Sunriver Resort (USA), 2011.

[9] A. Boëlle, G. Balzer and O. Simonin, Second-order prediction of the particle-phase stress tensor of inelastic spheres in simple shear dense suspensions, *In Gas-Particle Flows, ASME FED*, 228, 9-18, 1995.

[10] A. Gobin, H. Neau, O. Simonin, J. R. Llinas, V. Reiling and J. L. Selo, Fluid dynamic numerical simulation of a gas phase polymerization reactor, *Inter. Journal for Numerical Methods in Fluids*, Vol. 43, 1199-1220, 2003.

[11] N. A. Konan, H. Neau, O. Simonin, M. Dupoizat and T. Le Goaziou, Reactive Multiphase Flow Simulation of Uranium Hexafluoride Conversion Reactor*, In 7th International Conference on Multiphase Flow*, ICMF, Tampa, FL, May 30 - June 4, 2010a.

[12] A. Konan, H. Neau, O. Simonin, M. Dupoizat, T. Le Goaziou, 3D Unsteady Multiphase Simulation of Uranium Tetrafluoride Particle Fluorination in Fluidized Bed Pilot, In: G. Yue, H. Zhang, C. Zhao, Z. Luo (Eds.), *Proceedings of the 20th International Conference on Fluidized Bed Combustion,* Springer Berlin Heidelberg, 1152-1158, 2010b.

[13] R.S. Barlow, A.N. Karpetis, J.H. Frank, and J.-Y. Chen, Scalar profiles and no formation in laminar opposed-flow partially premixed methane/air flames, *Combustion and Flame*, 127, 2102-2118*,* 2001.

[14] W. L. Grosshandler, RADCAL: A Narrow-Band Model for Radiation Calculations in a Combustion Environment, NIST technical note 1402, 1993.

[15] H. Neau, P. Fede, J. Laviéville, and O. Simonin, High Performance Computing (HPC) for the Fluidization of Particle-Laden Reactive Flows, *14th International Conference on Fluidization – From Fundamentals to Products*, Eds, ECI Symposium Series, 2013.

[16] P. Pre, M. Hemati, B. Marchand, Study on natural gas combustion in fluidized beds: modelling and experimental validation, *Chem. Eng. Sci*., 53, 2871-2883, 1998.

[17] Web site of the International Workshop on Measurement and Computation of Turbulent Nonpremixed Flames (TNF), http://www.sandia.gov/TNF/radiation.html